Structure
Article

Dissecting the Kinematics of the Kinesin Step

Zhechun Zhang[1] and D. Thirumalai[1,2,*]
[1]Biophysics Program, Institute for Physical Science and Technology
[2]Department of Chemistry and Biochemistry
University of Maryland, College Park, MD 20742
*Correspondence: thirum@umd.edu
DOI 10.1016/j.str.2012.02.013

SUMMARY

Kinesin walks processively on microtubules in an asymmetric hand-over-hand manner with each step spanning 16 nm. We used molecular simulations to determine the fraction of a single step due to conformational changes in the neck linker, and that due to diffusion of the tethered head. Stepping is determined largely by two energy scales, one favoring neck-linker docking and the other, $\varepsilon_h^{MT\text{-}TH}$, between the trailing head (TH) and the microtubule. Neck-linker docking and an optimal value of $\varepsilon_h^{MT\text{-}TH}$ are needed to minimize the probability that the TH takes side steps. There are three major stages in the kinematics of a step. In the first, the neck linker docks, resulting in ~(5–6) nm movements of the trailing head. The TH moves an additional (6–8) nm in stage II by anisotropic translational diffusion. In the third stage, spanning ~(3–4) nm, the step is complete with the TH binding to the αβ-tubulin binding site.

INTRODUCTION

Molecular motors, such as myosin, kinesin, and dynein, which are involved in a number of cellular processes, walk along polar tracks ferrying cargo. Among the smallest motors is kinesin-1 (referred to as kinesin from here on), which is a cellular transporter that carries membrane organelles, mRNAs, and protein complexes along microtubules (MTs) (Block, 2007; Hirokawa et al., 2009; Vale, 2003). Kinesin contains two identical motor heads and takes hundreds of steps by walking in an asymmetric hand-over-hand manner (Yildiz et al., 2004; Asbury et al., 2003; Hua et al., 2002; Rice et al., 1999) on MTs before it detaches. In each step—spanning ~8.1 nm, the distance between two successive αβ-tubulin binding sites—kinesin goes through an ATP-driven reaction cycle (Figure 1A) that results in the alteration of the nucleotide-dependent interactions between the MT and the motor head. The processive hand-over-hand motion of the motor heads leads to cargo movement predominantly toward the MT plus end (especially at low loads), through a coiled coil and cargo-binding domain that link the heads and the cargo (Kozielski et al., 1997; Vale and Milligan, 2000). A common theme in the motility of all motors is binding, release from the polar tracks, and subsequent rebinding of the motor head to the target binding site (TBS) (Spudich and Sivaramakrishnan, 2010; Vale, 2003). These processes, which result in a single step fueled by ATP consumption, involve not only coordination between the motor heads but also allosteric communication between the motor heads and regions of the polar track spanning several nanometers.

A number of remarkable studies (Spudich and Sivaramakrishnan, 2010; Kolomeisky and Fisher, 2007; Gennerich and Vale, 2009; Schief and Howard, 2001; Carter and Cross, 2006; Block, 2007) have been used to unravel the stepping mechanisms of motors (especially kinesin and myosin). Of particular relevance here are single-molecule experiments with kinesin (Carter and Cross, 2005; Yildiz et al., 2008; Guydosh and Block, 2006; Asbury et al., 2003; Svoboda et al., 1993), which have provided considerable insight into the global processes that power the trailing head (TH) toward the microtubule (+) end. Single-molecule measurements of the time-dependent changes in the cargo attached to the coiled coil show that the motor head jumps between the tubulin-binding sites on a timescale that is much shorter than the waiting time between steps (Yildiz et al., 2004). In order to reveal the molecular changes that occur during the jump time, which are difficult to quantify using experiments alone, we have simulated the kinematics of a single step using a coarse-grained model for the MT-kinesin complex. The new model and Brownian dynamics simulations with hydrodynamic interactions are used to answer the following questions: (1) What fraction of a single step is associated with the energetically favored conformational transitions that are linked to the power stroke? (2) How far does the trailing head move by tethered diffusion? (3) What are the key interactions that propel the TH to move predominantly parallel to a single protofilament of the MT?

Although the MT usually contains 13 protofilaments, kinesin walks on a single protofilament under normal operating conditions (Ray et al., 1993; Block et al., 2003; Yildiz et al., 2008). During a single step, the TH detaches from the initial αβ-tubulin binding site (the circle with hash marks in Figure 1B), passes the MT-bound leading head (LH), and reattaches to the target αβ-tubulin binding site 16 nm away on the same protofilament (Figures 1A and 1B). The target binding site (shown in green in Figure 1B), however, is just one of several accessible αβ-tubulin binding sites along the 16 nm trip (Figure 1B). Some of the potential binding sites on the curved MT surface are too far away for the TH to access them (Figure 1B). However, the sites marked in pink and red can be reached by stretching the neck linker (NL) but are largely avoided during the stepping process. It has been proposed that the conformational change from a disordered to an ordered state in the neck linker upon docking to the LH propels the TH toward the (+) end of the MT, and hence can be considered to be the power stroke (Rice et al., 1999;

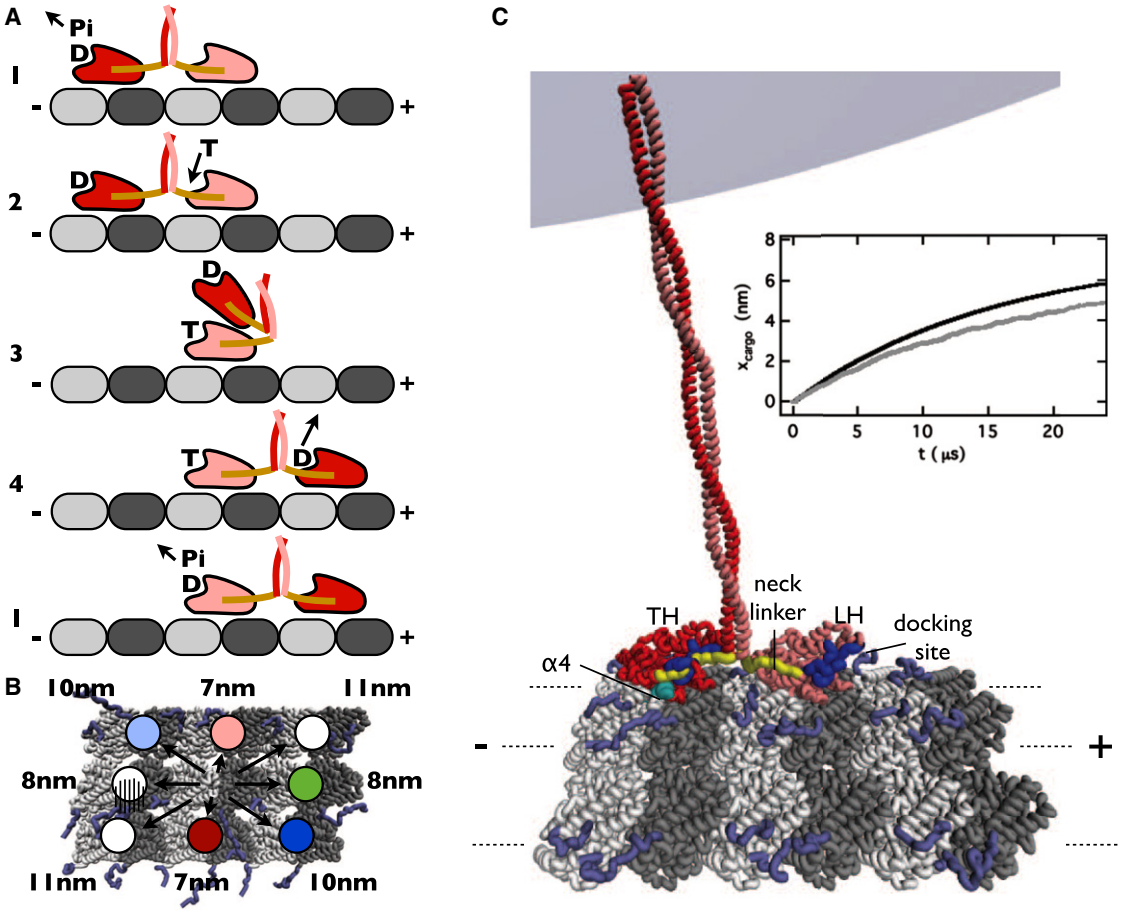

Figure 1. Simulation Setup and Validation

(A) Catalytic cycle of kinesin. The trailing head (TH) is shown in red and the leading head (LH) is in pink. ATP, ADP, and Phosphate are represented by T, D, and Pi, respectively. Binding of ATP, release of ADP, and Pi are indicated by incoming and outgoing arrows.

(B) Distances to the various binding sites from the central location corresponding to the bound LH. The distances are between the centers of the binding sites. Pink and red circles are potential sites to which the TH can bind based on the geometry of the MT-Kin complex.

(C) The structural model of the complex used in the simulations; α- and β-tubulin are in silver and gray, respectively, and are augmented by ehooks (violet). The TH is in red, and the LH is shown in pink. The neck linker is shown in yellow, and its docking site is in blue. Part of the 500 nm cargo is also shown. The microtubule binding the α4 helix of the TH is in cyan. The top right panel shows the average cargo movement along the MT axis during single 8 nm steps under a 5 pN resisting load obtained using simulations (gray line). The corresponding experimental result from Carter and Cross (2005) is shown in black. Good agreement between simulations and experiment validates the model.

See also Figure S1.

Tomishige et al., 2006). The neck linker (shown in yellow in Figure 1C) is a peptide containing ~13 residues that connects the motor heads to the N-terminal of the coiled coil (the dimerization domain). When both heads are bound to the MT, the LH neck linker extends backward and does not interact with the rest of the LH (Tomishige et al., 2006). Upon ATP binding to the LH, the neck linker undergoes a conformational change (Rice et al., 1999; Tomishige et al., 2006; Rosenfeld et al., 2001; Skiniotis et al., 2003; Asenjo et al., 2006; Hwang et al., 2008; Khalil et al., 2008) and extends forward and docks to the cover strand and the central β sheet of the LH. Such a conformational change (disorder → order transition) results in undocking and docking of the NL, which plays a crucial role in detaching the TH from the MT and propelling it toward the (+) end of the MT as it searches for and locates the TBS.

A number of observations suggest that conformational changes in the neck linker are necessary for the stepping kinetics of kinesin. First, immobilization of the neck linker by crosslinking it to the motor domain inhibits kinesin motility (Tomishige and Vale, 2000). Second, disfavoring neck-linker docking decreases the stall force (Khalil et al., 2008). Third, replacement of the neck linker by extended or flexible peptide impairs coupling between ATP turnover and the 16 nm step (Yildiz et al., 2008; Clancy et al., 2011). Finally, the strain in the neck linkers serves as a gating mechanism so that the two heads can operate out of phase to execute the observed processive motion (Guydosh and Block, 2006; Yildiz et al., 2008; Block, 2007). However, the adequacy of the neck-linker docking model as the sole structural basis for explaining the stepping mechanism has also been questioned (Schief and Howard, 2001; Block, 2007), in part because

the length of a fully stretched neck linker is short of the 16 nm distance between the initial and the target binding sites (Block, 2007). In addition, it is still unclear how much of the energy released during ATP binding is used to trigger neck-linker docking (Block, 2007; Hackney, 2005; Rice et al., 2003). Thus, the consequences of neck-linker docking, which appears to be the most visible conformational change during the kinesin step, occurring on a timescale of tens of μs, have not been revealed at the molecular level.

In this study, we provide a comprehensive view of the molecular events during kinesin stepping using simulations based on a coarse-grained model that is the first of its kind, to our knowledge. We explore the link between neck-linker docking, directed diffusion, and the strength of interaction between the TH and the microtubule in relation to the kinematics of the kinesin step. Our simulations quantify the fraction of the step from the power stroke (NL docking) and due to the tethered diffusion, which have proved difficult to resolve using experiments, because the jump times (tens of μs) are considerably shorter than the time between steps. We show that although NL docking results in only (5–6) nm movement of the TH along the microtubule, it not only prevents reattachment to the starting site but also is essential in minimizing the probability of taking side steps at an optimum value of interaction strength between the motor head and the MT. By performing a number of mutation simulations we find, in accord with experiments (Yildiz et al., 2008), that enhancing the flexibility of the neck linker results in increased probability of taking side steps. Our results show that the stepping kinetics occurs in three major stages, the first of which is neck linker docking, which poises the TH to move predominantly toward the (+) end along a single protofilament of the microtubule. In the second stage, the TH undergoes tethered directed diffusion, characterized by anisotropic translational motion but isotropic rotation. Surprisingly, a substantial fraction of the step occurs during this stage. Finally, optimal interaction between the microtubule and the TH is required to complete the step with minimal probability of taking side steps, which highlights the important role that the microtubule plays in facilitating the directed motion of the motor head.

RESULTS AND DISCUSSION

In order to explore the roles of neck-linker docking to the leading head and the interaction between the TH and the MT binding sites in the stepping process, we performed a variety of simulations. The details of the simulations are in Table S1 available online. The two key parameters that control the kinematics of kinesin stepping are $\varepsilon_h^{LH\text{-}NL}$, the strength of interaction between the residues in the neck linker and those in the LH, and $\varepsilon_h^{MT\text{-}TH}$, measuring the strength of interaction between the TH and potential binding sites on the MT (see Equation 1 in the Supplemental Information, describing the force field). Docking of the NL to the LH is favorable only if $\varepsilon_h^{LH\text{-}NL}$ exceeds a threshold value (see below). Further increase in $\varepsilon_h^{LH\text{-}NL}$ makes neck-linker docking more favorable. Similarly, increase of $\varepsilon_h^{MT\text{-}TH}$ results in stronger affinity between the TH and the MT binding sites. Most of the results presented correspond to $\varepsilon_h^{LH\text{-}NL}$ = 2.0 kcal/mol, resulting in rapid docking, and $\varepsilon_h^{MT\text{-}TH}$ = 0.2 kcal/mol, for which the probability of the TH taking side steps is minimal. We also varied both $\varepsilon_h^{LH\text{-}NL}$ and $\varepsilon_h^{MT\text{-}TH}$ to ascertain their effects on the kinematics of a single step.

Simulated Cargo Movement under a Resistive Load Compares Well with Experiment

To validate the model (see Figure S1 for the structure of the complex) and the simulation strategy, we first calculated the movement of the cargo when a resistive force is applied in the (−) direction of MT (Figure 1C). The resulting setup (Figure 1C) mimics the experimental conditions used by Carter and Cross (2005), who found, by monitoring the time-dependent changes in the cargo position, $x_{cargo}(t)$, that if the resolution time exceeds ~25 μs, the cargo moves by ~8.1 nm without taking substeps. The calculated $x_{cargo}(t)$ for a 500 nm cargo, averaged over 99 trajectories, under a resistive load of 5 pN is in good agreement with experiments (Figure 1C, top right). Our simulation results can be fit using $x_{cargo}(t) = A(1 - e^{-t/\tau_c})$, where A = 6.4 nm and τ_c = 16.6 μs. The values of A and τ_c obtained in experiments (Figure 1C, top right, black line) are 7.4 nm and 15.3 μs, respectively (Figure 3 in Carter and Cross [2005]), which shows that our simulations capture the global features of the mechanics of a single kinesin step.

Trailing Head Moves ~6 nm upon Neck-Linker Docking

In order to dissect the molecular events during the stepping process, we focused on the consequences of docking of the NL to the LH. From the distribution of first passage times for the NL to dock to the LH, calculated from (100–200) trajectories for which ordering is complete (Equation 1 in Experimental Procedures), the mean NL docking time $\langle\tau_{NL}\rangle$ ranges from 0.10 to 0.39 μs (see Table S1), depending on $\varepsilon_h^{LH\text{-}NL}$. During docking of the NL, the vector connecting the N and C termini of the NL of the LH (referred to as LH-NL), which initially points toward the (−) end of the MT (Figure 2A, top), undergoes an ~180° rotation and is directed toward the MT (+) end (Figure 2A, middle structure). Concurrently, the TH detaches from the initial binding site. The location of the center of mass of the TH at the instant when NL docking is complete is displayed in Figure 2B. The distribution, $P(x_{TH}^d)$, of x_{TH}, the distance traveled by the center of mass of the TH along the MT axis (x axis), calculated from the data in Figure 2B, shows that upon completion of NL docking, the mean $\langle x_{TH}^d\rangle$ = 5.2 ± 0.1 nm (Figure 2C), which is ~11 nm shy of the TBS. The small value of $\langle x_{TH}^d\rangle$ can arise because movement of the TH lags behind NL docking to the LH. We rule out such an explanation, because the C-terminal residue T338 of the LH-NL moves only 6.0 ± 0.01 nm along the MT when NL docking is complete (Figure 2C). Thus, NL docking and the movement of the center of mass of the TH are almost synchronous.

The nature of diffusive motion of the TH can be gleaned from the time dependence of x_{TH}, $x_{TH}(t)$, in a sample trajectory shown in Figure 2D. In this trajectory, $x_{TH}(t)$ rises sharply, reaching ~6 nm upon completion of docking. Subsequently, the TH undergoes diffusive motion until the step is complete. The diffusion time (~20 μs in Figure 2D), which varies from trajectory to trajectory, is in the range (10–30) μs. These observations suggest that a large fraction (~0.6) of the total step occurs by stochastic search for the TBS, and not merely due to the power stroke generated by conformational changes in the neck linker.

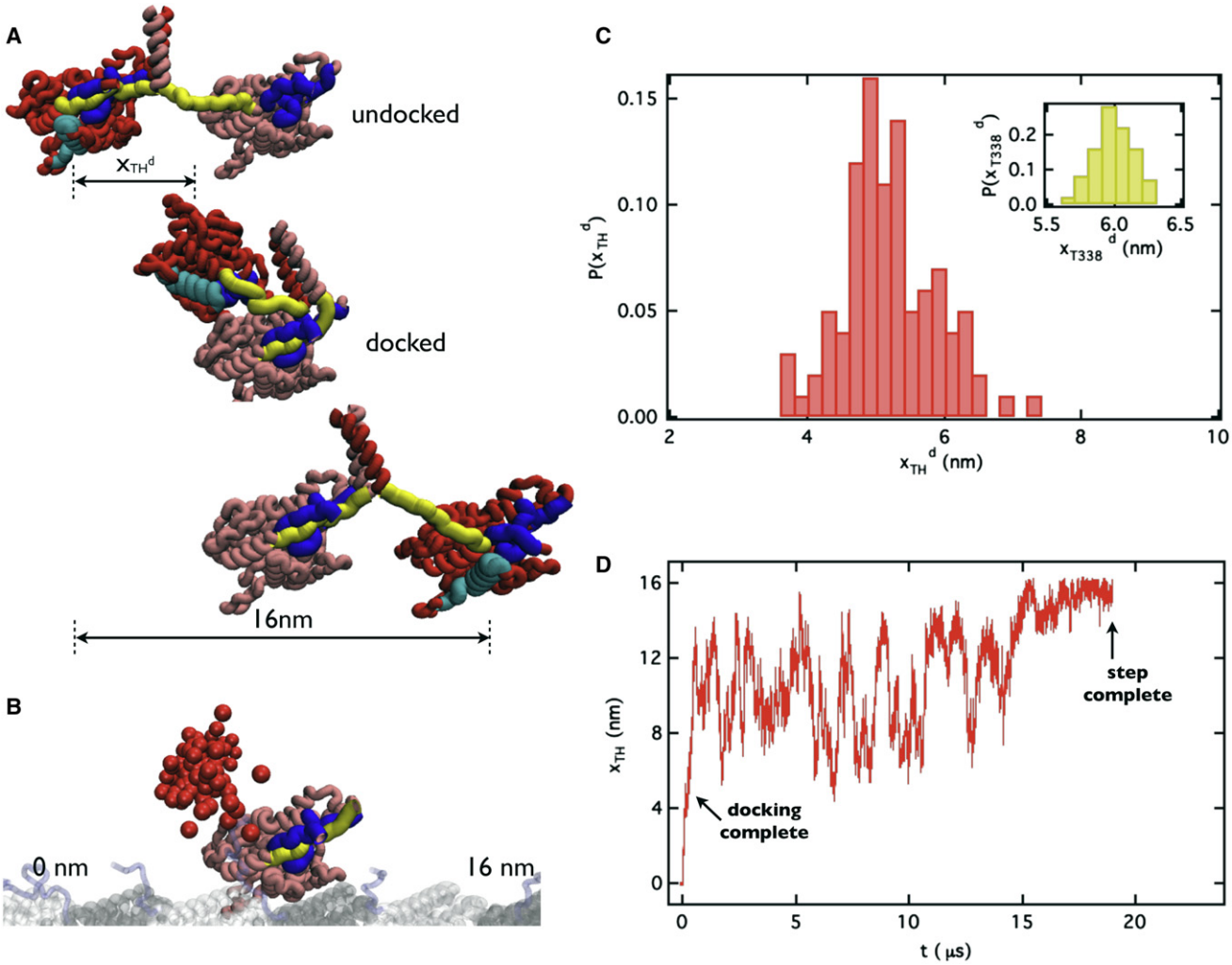

Figure 2. Dynamics of Neck-Linker Docking

(A) The LH and TH at the beginning (top) and end (middle) of neck-linker docking to the LH, and at the end of a 16 nm step (bottom) in a representative trajectory. The center-of-mass displacement of the TH along the microtubule axis during neck-linker docking is x_{TH}.

(B) Location of the TH (red sphere) from 99 trajectories when neck-linker docking to the LH is complete.

(C) Histograms, based on 99 trajectories, of the TH movement (red) during neck-linker docking to the LH. The inset shows distributions of the position of T338 of the LH.

(D) Time-dependent changes in the center of mass of the TH as a function of t for a sample trajectory. The arrow shows that NL docking is complete in ~1 μs and the stepping time is ~20 μs. The values of $\varepsilon_h^{LH\text{-}NL}$ and $\varepsilon_h^{MT\text{-}TH}$ are equal to 2.0 and 0.2 kcal/mol, respectively.

See also Table S1 and Movie S1.

To further confirm that NL docking does not lead to completion of a full step, we performed several additional simulations by altering the key parameters in the force field (see Table S1). These simulations, in which (100–200) trajectories were generated for several force-field parameters (variations in $\varepsilon_h^{LH\text{-}NL}$ and $\varepsilon_h^{MT\text{-}TH}$, and changes in the dielectric constant of the electrostatic interactions) also show that upon completion of NL docking, the TH step is incomplete (detailed in Table S1). Besides establishing the robustness of the results to changes in the force-field parameters, the complete set of results shows that NL docking alone, without directed diffusion, is insufficient to drive the TH to the neighborhood of the TBS (Block, 2007; Carter and Cross, 2006).

Minimizing the Probability of Side Steps Requires NL Docking and Optimal Interaction between the Motor Head and the MT

How are side steps largely avoided, even though they are within easy access of the TH? To answer this question, we considered the possibility that NL docking and appropriate interactions with the MT reduce the probability that the TH will bind to αβ-tubulin binding sites on MT (pink and red circles in Figure 1B). From geometrical considerations alone, it appears that NL docking to the leading head (Figure 1B) restricts the TH from reaching several sites (white and light blue circles in Figure 1B) even if the NL of the TH is fully stretched. However, Figure 1B also shows that even after NL docking, the sites that are above and

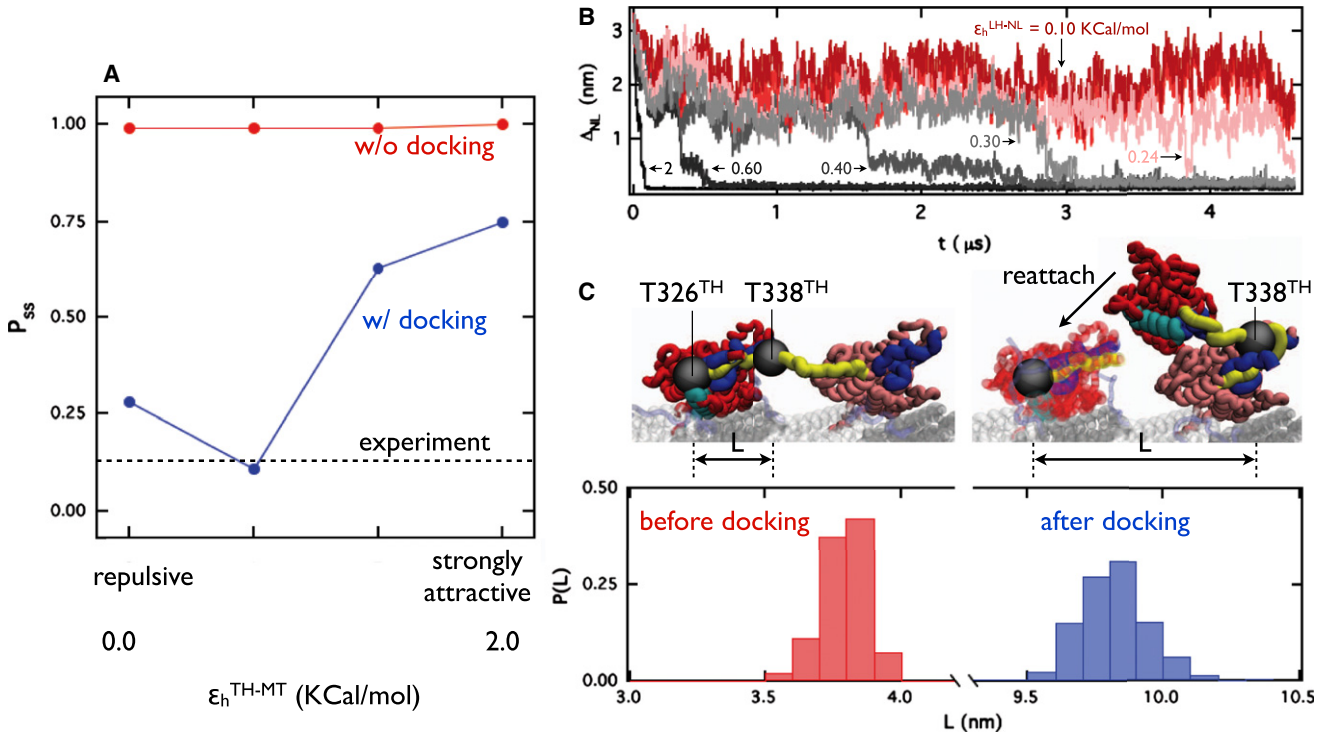

Figure 3. Consequences of Neck-Linker Docking

(A) Probability of side steps, P_{ss}, as a function of MT-TH interaction. Repulsive, weakly attractive, attractive, and strongly attractive corresponds to ε_h^{MT-TH} (Equation 1 in the Supplemental Information) values of 0.0, 0.2, 0.4, and 2.0 kcal/mol, respectively. The dotted line corresponds to the probability, observed in experiments, that the TH takes side steps in wild-type kinesin (13%) (Yildiz et al., 2008).

(B) Time-dependent changes in $\Delta_{NL}(t)$, the measure (Equation 1) used to assess the extent of docking of the NL to the leading head as a function of ε_h^{LH-NL}. The curves in various shades of gray show that docking is complete ($\Delta_{NL}(t) < \Delta c$), while those in pink and red show that $\Delta_{NL}(t) > \Delta c$.

(C) The structure on the left shows the locations of T326 and T338 in the TH bound to the initial binding site. The distance between these residues is less than 4 nm. The structure on the right shows the location of TH T338 after NL docking to the LH, and the location of TH T326 assuming the TH reattaches to the initial binding site. The bottom panel shows the distributions of $|\vec{R}^{TH}_{T338}(0) - \vec{R}^{TH}_{T326}(0)|$ (red) and $|\vec{R}^{TH}_{T338}(\tau_{NL}) - \vec{R}^{TH}_{T326}(0)|$ based on 200 trajectories, where τ_{NL} is the time at which NL docking to the LH is complete in a trajectory.

See also Movie S2.

below the central binding site (pink and red circles in Figure 1B) to which the LH is anchored are accessible, as they are within reach of the stretched NL of the TH. Thus, favorable energetics must bias the TH so that the TBS is reached with substantial probability within the typical stepping time of ~25 μs.

We surmise that the motor head is correctly bound to the TBS if the structure is similar to that found in the cryoEM-image of Kin-MT complex (Sindelar and Downing, 2007), which implies that both the distance and orientational criteria (Equations 3, 4, and 5) must be simultaneously satisfied. Incorrect binding would lead to side steps, which is realized by the TH binding to αβ-tubulin on neighboring protofilaments (red, pink, or dark blue circle in Figure 1B), occurring in the same manner as steps to the TBS. In order to provide structural details of how NL docking to the LH prevents side steps, we performed simulations using a mutant in which NL docking is made energetically unfavorable (ε_h^{LH-NL} = 0) so that docking is prevented (see Supplemental Information for details). Such a construct may be realized in experiments either by deleting the cover stand (Hwang et al., 2008; Khalil et al., 2008) or by replacing the NL with glycine-serine repeats (Yildiz et al., 2008).

Consequences of NL Docking

We find that minimizing the probability of taking side steps requires optimal values of ε_h^{MT-TH} and docking of NL to the LH, which requires that ε_h^{LH-NL} exceed a threshold value (see below). Figure 3A shows that in the absence of NL docking to the LH (ε_h^{LH-NL} = 0), the probability of the TH taking a 16 nm step by binding to the TBS is zero, independent of ε_h^{MT-TH}. For ε_h^{LH-NL} = 2.0 kcal/mol, the docked NL is almost intact on the timescale of a single step, thus preventing the detachment of the TH from the MT. The mean docking time, $<\tau_{NL}>$, increases from about 0.10 μs to a value greater than 3.7 μs as ε_h^{LH-NL} decreases from 2.0 kcal/mol to 0.4 kcal/mol. Further decrease in ε_h^{LH-NL} makes NL docking unfavorable. Figure 3B shows that if ε_h^{LH-NL} decreases below 0.3 kcal/mol, then NL does not dock in a stable manner, as assessed by $\Delta_{NL}(t)$ (Equation 1), even on timescales on the order of ~5 μs.

Comparison of the wild-type (WT) and mutant simulations shows that NL docking to the LH is largely responsible for ensuring that the TH moves with substantial probability toward the target binding site. Besides decreasing the probability of side steps (see below), NL docking to the LH also prevents

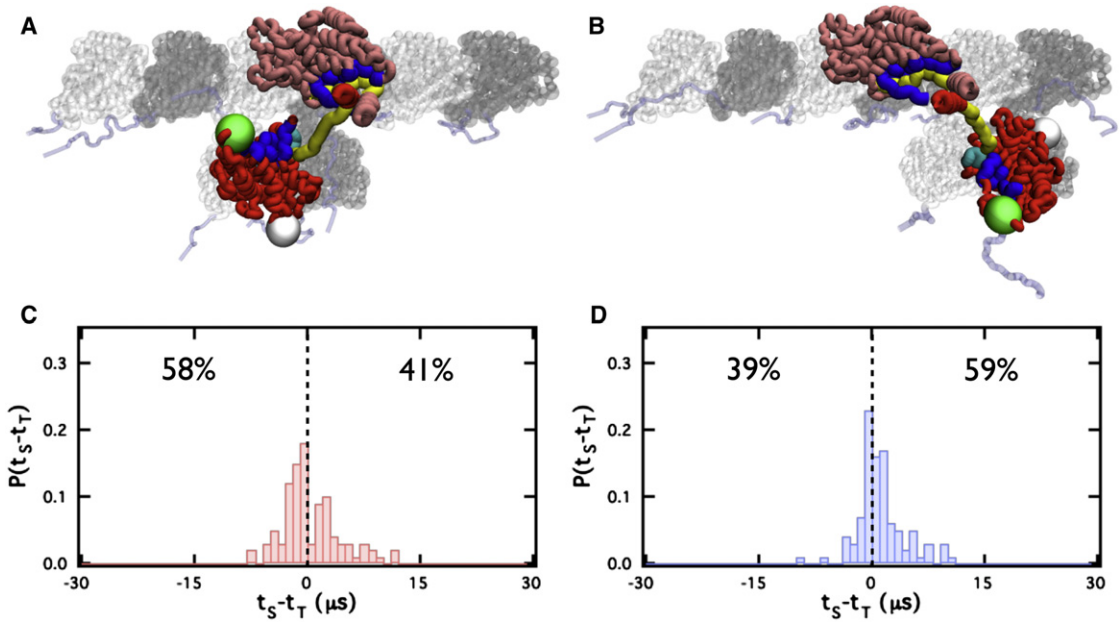

Figure 4. Transient Visits of TH to Sites on the Neighboring Protofilament

(A) Conformation showing that the TH transiently visits the binding site below the LH (the red site in Figure 1B).

(B) Same as (A), except that the TH visits the binding site below the target (the dark blue site in Figure 1B).

(C) Distributions of $t_S - t_T$ for 100 trajectories generated in simulations where the probability of taking steps is minimal (see Figure 3A). Here, t_S is the time at which the TH first enters the neighborhood of the binding site in (A), while t_T is the corresponding time for reaching the TBS.

(D) Same as (C), except that t_S is the first passage time for the binding site shown in (B).

See also Figure S2.

rebinding of the TH to the initial binding site. In order to demonstrate this particular consequence of NL docking, we first calculated the distribution P(L), where $L = |\vec{R}^{TH}_{T338}(0) - \vec{R}^{TH}_{T326}(0)|$ (Figure 3C) is the distance between T338 and T326 of the TH neck linker at t = 0. At t = 0, P(L) peaks at ~3.8 ± 0.05 nm (red in Figure 3C), which is the equilibrium value of L when the motor head is bound to the initial αβ-tubulin binding site. In contrast, the distribution of $|\vec{R}^{TH}_{T338}(\tau_{NL^i}) - \vec{R}^{TH}_{T326}(0)|$, where i labels the ith trajectory (Figure 3C), peaks around 9.8 nm (blue in Figure 3C). Thus, once docking is complete, resulting in tension in the leading head NL (see below), the detached TH is too far away from the initial binding site, so that rebinding cannot occur provided $\varepsilon_h^{LH\text{-}NL}$ is sufficiently large. At small values of $\varepsilon_h^{LH\text{-}NL}$, however, NL docking is reversible (Figure 3B), which could result in the TH binding to the initial binding site.

Effect of $\varepsilon_h^{MT\text{-}TH}$

The majority of side steps observed in the mutant simulations correspond to the TH binding to the middle αβ-tubulin on the right protofilament adjacent to the LH-bound αβ-tubulin on the central protofilament (Figures 1B and 4A), even though the pink circle is at the same distance as the red site (Figure 1B). In a small fraction of trajectories, the TH is trapped in other binding sites with correct orientation. This result suggests that diffusion alone, without any additional biasing mechanism favoring the target binding site, cannot explain the observation that kinesin walks predominantly on a single protofilament under normal operating conditions (Ray et al., 1993; Block et al., 2003; Yildiz et al., 2008). The probability of taking side steps, P_{ss} (Equation 6), depends on $\varepsilon_h^{MT\text{-}TH}$ (blue lines in Figure 3A), even when NL docking is highly favorable, $\varepsilon_h^{LH\text{-}NL}$ = 2 kcal/mol. When the MT-TH interaction is strong ($\varepsilon_h^{MT\text{-}TH}$ = 2 kcal/mol), only 25% of the trajectories locate the TBS. The remaining trajectories are kinetically trapped in adjacent αβ-tubulin sites (Figures 4A) for timescales exceeding ~25 μs, with the kinesin-MT interface formed only partially. As $\varepsilon_h^{MT\text{-}TH}$ decreases, P_{ss} decreases dramatically, reaching a minimum at ~0.11 (Figure 3A), which is remarkably close to the experimental estimate for the wild-type (Yildiz et al., 2008). Movie S1 shows the sequence of events in a trajectorythat makes a correct step, and one with an incorrect step is shown in Movie S2. Our findings support the conclusion that rapid disorder → order transition of the leading-head neck linker decreases the probability of side steps (Hyeon and Onuchic, 2007a). The dependence of P_{ss} on $\varepsilon_h^{MT\text{-}TH}$ suggests that maximizing the probability of TH binding to the TBS requires robust NL docking ($\varepsilon_h^{LH\text{-}NL}$ should exceed a threshold value for docking to be favorable) as well as relatively weak MT-TH interaction. These results further imply that ADP release, which would result in an effective increase in $\varepsilon_h^{MT\text{-}TH}$, should occur late in the stepping process. Thus, besides ensuring that the TH predominately moves toward the (+) end of the MT, docking of the NL decreases the probability of long-lived side steps, provided $\varepsilon_h^{LH\text{-}NL}$ and $\varepsilon_h^{MT\text{-}TH}$ are in the appropriate ranges.

Trailing Head Visits Binding Sites in the Adjacent Protofilament of the MT

In order to show that the TH transiently visits sites in the neighboring protofilament (notably the red and dark blue sites in

Figure 1B) even when NL docking is highly favorable, we calculated that for each trajectory t_S, the time at which the TH first enters the neighborhood of binding sites (ΔTH in Equation 7 should be less than 4 nm), and t_T, the time at which the TH locates the TBA. If transient side steps are common (Figure 4A), we expect values of $t_S < 30$ μs (the length of our simulation) in the majority of the trajectories. In addition, if the TH takes transient side steps before reaching the TBS, we expect $t_S < t_T$.

The distributions of t_S (Figure 4B) for reaching the red and blue binding sites (Figure 1B) show that in almost all the trajectories, t_S is less than 30 μs (99% for the red binding site and 98% for the blue). In 58% of these trajectories, the TH visits the red binding site (the binding site below the LH shown in Figure 4A) before reaching the target. In 41% of the trajectories, the TH visits the TBS first and then hops to the binding site below the LH. For the blue binding site (the one below the target shown in Figure 4B), the corresponding probabilities are 39% and 59%. The finite probability of the TH visiting the red and blue sites after reaching the target suggests that the TH may hop between these binding sites on the protofilament during the 16 nm step. Because such events occur on timescales shorter than the duration of a single step, they may be hard to characterize experimentally. Transient hopping to the sites in Figure 4A, which are accessible with appropriate stretching of the NL, shows that there is inherent randomness in the jump kinetics associated with the stepping process (see also Figure 2D).

Flexibility of Disordered NL of the LH Results in Side Steps

Time-dependent changes in $R_y(t) = \hat{e}_y \cdot (\vec{R}^{TH}_{T326}(t) - \vec{R}^{LH}_{T326}(t))$, the total extension of TH-NL and LH-NL projected along the y axis that is perpendicular to the central protofilament, for a sample trajectory, illustrate that the docking state of the NL determines the probability of taking side steps (Figure 5). From the geometry of the MT (Figure 1B), it follows that for a side step with correct orientation, Ry (Figure 5A) should extend by at least ~6 nm (Figure 5B). Thus, both TH and LH neck linkers must extend to account for the needed ~6 nm. Because the NL of the trailing head is disordered and hence flexible, it can make sideways excursions readily. The probability of the NL of the LH extending sideways greatly depends on its docking state (Figure 5). Upon docking, sideways movements of the NL are strictly prohibited (see the gray lines in Figure 5) whereas they can occur if docking is energetically unfavorable (black lines in Figure 5), which we mimic with $\varepsilon_h^{LH\text{-}NL} = 0$ Kcal/mol. Comparison of Figures 5B–5D shows that if the TH takes side steps, then the NL of the LH should extend sideways by ~4 nm, while the more flexible NL of the TH should extend sideways by ~2 nm. Thus, as long as the NL of the LH is docked ($\varepsilon_h^{LH\text{-}NL}$ exceeds a threshold value), even with the full extension of the NL the TH cannot take side steps readily (gray lines in Figure 5), especially when MT-TH interaction is weak. These calculations provide a structural explanation of why the WT kinesin appears to walk predominantly along a single protofilament under normal operating conditions (Ray et al., 1993; Block et al., 2003) on timescales exceeding ~25 μs.

Estimation of Tension in the Neck Linker

Several experiments have shown (Guydosh and Block, 2006; Yildiz et al., 2008) that communication between heads occurs by mechanical strain within the kinesin molecules. Such a gating mechanism is due to transmission of tension in the NL of the motor heads when they bind to the MT. Simulations have shown that the mean tension in the NL when both heads are bound to the MT is ~(15–30) pN (Hyeon and Onuchic, 2007b; Hariharan and Hancock, 2009). The equilibrium distribution $P(x_{NL})$ of the extension, x_{NL}, projected along the MT axis of the NL when both heads are bound to the MT (Figure 6A) shows that the neck linkers are stretched and hence are under strain. The extensions of the neck linkers during the stepping process have not been previously characterized. The distribution $P(x_{NL})$ of the NL docked to the LH shows that it peaks around 3.5 nm (Figure 6B), with relatively small dispersion. On the other hand, the $P(x_{NL})$ of the TH is broad, with a peak at x_{NL} ~2.8 nm. The corresponding distribution of the angle made by the vector connecting T326 and T338 of the NL and the MT axis (θ_{NL}) shows (Figure 6C) that for the TH, it peaks around the value of ~30°, corresponding to the value in the crystal structure. In contrast, $P(\theta_{NL})$ for the TH is broad, indicating considerable orientational disorder, consistent with the diffusive nature of TH motion. From the results in Figure 6B, we calculated the forces needed to stretch the neck linkers assuming that they can be characterized as worm-like chains. The resulting distributions of tension in the neck linkers show (Figure 6D) that the average tension in the NL of the LH is ~31.1 pN, with dispersion of ~10.5 pN. The corresponding value for the NL of the TH is ~15.4 pN, with a large dispersion of ~12.2 pN. It might seem surprising that the estimated mean values of tension in the neck linker during the stepping process exceed the stall force of ~7 pN. However, the precise value of the force at the interface of the motor head and the MT in response to tension in the NL can be considerably less and is determined by how strain is transmitted through the architecture of the motor head.

Binding to the Target Site on the MT Occurs in Three Major Stages

Attachment to the TBS involves three distinct stages: NL docking to the LH, followed by anisotropic directed diffusional search, and finally by recognition and binding to the TBS with correct orientation (see Figure 7A). In these simulations, we set $\varepsilon_h^{LH\text{-}NL}$ = 2.0 kcal/mol but varied $\varepsilon_h^{MT\text{-}TH}$. We monitored the progress of the stepping process using d(t) and the two angles θ_1 and θ_2 (Equations 3, 4, and 5), which specify the orientations of the TH, as order parameters to assess binding of the TH to the TBS. The values of d, θ_1, and θ_2 are ≈0 when TH is correctly bound to the TBS.

The TH reaches the neighborhood (d ≈ 4 nm) of the TBS by an anisotropic diffusive process in a few μs depending on $\varepsilon_h^{TH\text{-}MT}$. In analyzing the dynamics in the second stage, we used only the portion of the trajectories after NL docking is complete and prior to the TH reaching the neighborhood (d ≈ 4 nm) of the MT (gray regions in Figures 7B–7D). The diffusion coefficients, calculated from the slopes of the mean-square displacements along the x, y, and z components of the center of mass of the TH, yield $D_x \approx D_y \approx 15\ \mu m^2/s$ (Figure S2), whereas linear transport perpendicular to the MT surface is slow, with $D_z \approx 3\ \mu m^2/s$. In contrast, the isotropic translational diffusion coefficient of the TH using Hydropro (García De La Torre et al., 2000) is $D_x = D_y = D_z = D_{iso} \approx 26\ \mu m^2/s$. The TH also undergoes rotational

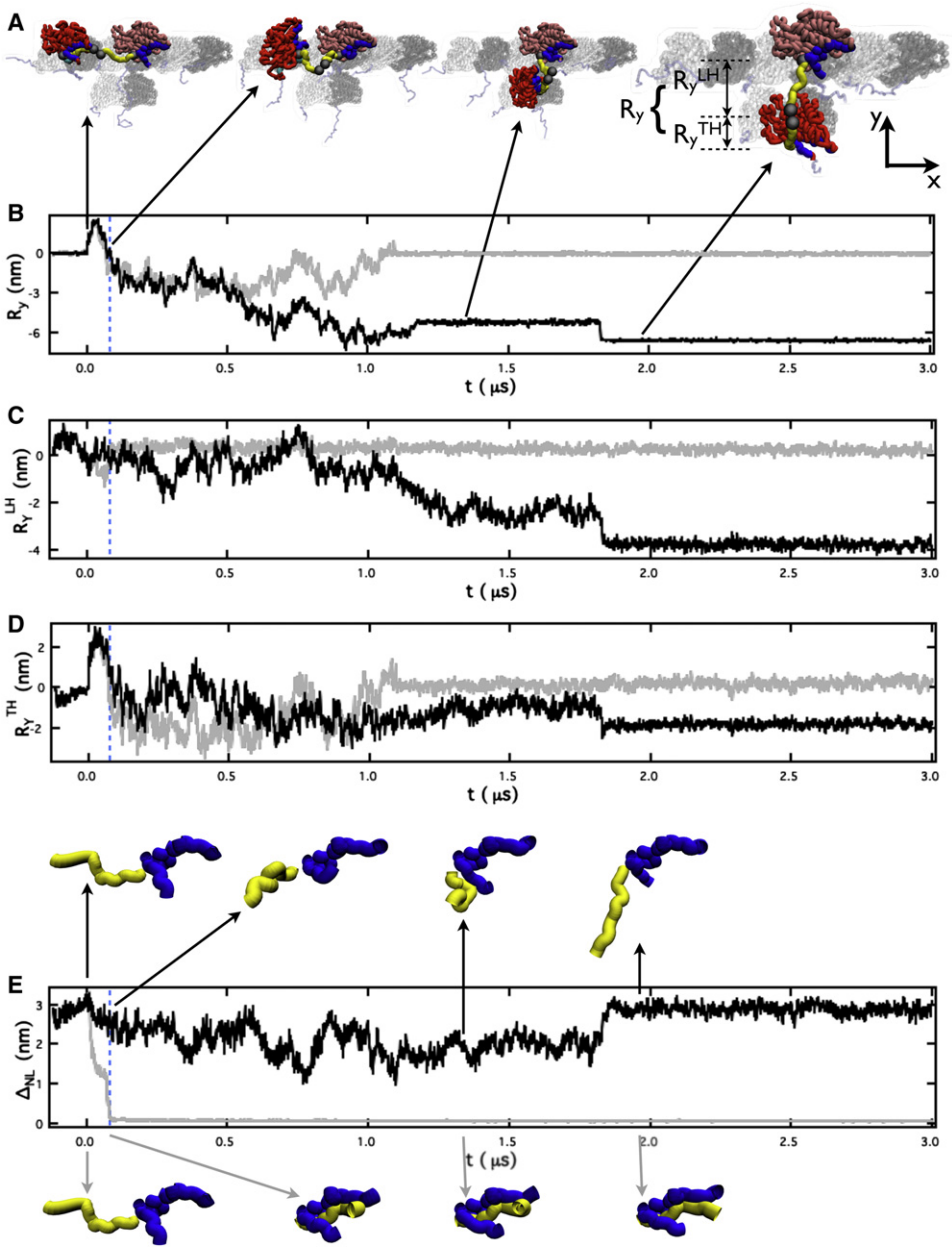

Figure 5. Flexibility of the Disordered NL of the LH Leads to Side Steps

(A) Four sequential snapshots in a representative trajectory, in which the TH binds to the middle αβ-tubulin on the adjacent protofilament corresponding to the red circle in Figure 1B. It shows (1) the beginning of a step, (2) detachment of the TH from the initial binding site, (3) interaction of the TH with tubulin on the neighboring site, and (4) binding of the TH to the tubulin with correct orientation.

(B) Ry(t) is the total extension of the TH-NL and the LH-NL projected along the y axis as a function of time for a normal 16 nm step (gray). The black line, corresponding to NL docking being unfavorable, shows that a side step requires a minimum of ~6 nm extension.

(C) $R_y^{LH}(t) = \hat{e}_y \cdot (\vec{R}_{T338}^{LH} - \vec{R}_{T326}^{LH})$, the extension of LH-NL projected along the y axis as a function of time, shows that a side step requires ~4 nm of side extension from LH-NL (black line).

(D) Same as (C), except this gives the contributions due to stretching of the TH to Ry(t) when NL docking is favorable (gray line) and unfavorable (black line).

(E) $\Delta_{NL}(t)$ (defined in Equation 1), the distance between LH-NL and LH, is plotted as a function of time for both favorable (gray) and unfavorable docking (black). Conformations of the NL of both the TH and LH at various instances are given. The results represented by gray and black lines in (B)–(E) were computed using $\varepsilon_h^{LH\text{-}NL}$ = 2.0 and 0.0 kcal/mol, respectively. The value of $\varepsilon_h^{MT\text{-}TH}$ was set to 2.0 kcal/mol.

diffusion (Figures 7B–7D), which unlike translational diffusion is essentially free. The isotropic rotation time constant is $\tau_R \approx$ 0.28 μs, obtained from the decay of the orientational autocorrelation function (see Figure S2), and the corresponding value from Hydropro (García De La Torre et al., 2000) is ~0.21 μs. These results show that the second stage, constituting the major

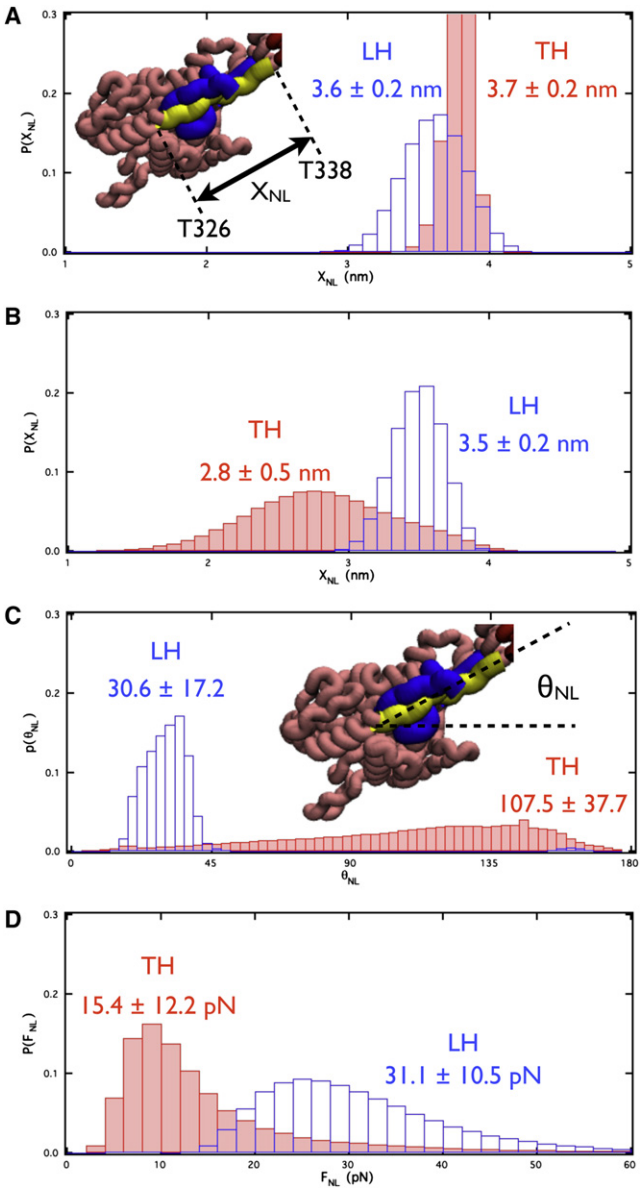

Figure 6. Distribution of Extension and Tension in the Neck Linkers

(A) Equilibrium distributions (t = 0) of the extension x_{NL}, the distance between the residues T326 and T338 projected along the MT axis, with both heads bound to the MT.

(B) Distributions of the extension x_{NL} obtained at the instant the NL of the LH is docked. The mean extension and the dispersion values are also given.

(C) Same as (B), except this panel gives the distributions of the angle, θ_{NL}, between the vector joining T326 and T338 and the x axis of the MT. In the docked state, the distribution (blue) peaks around the value found in the crystal structure.

(D) Calculation of the distribution of tension in the LH (blue) and the TH (red) using the results in (B) with the assumption that the NL can be treated approximately as a worm-like chain. The force extension relation and the values of the persistence length (lp) and the contour length (L) are also given. The accepted value of lp for polypeptides is in the range 0.5–0.7 nm; L = 0.38(NR − 1) nm, where NR = 13. Note that estimation of tension using the worm-like chain model is extremely sensitive to $p = x_{NL}/L$, especially when P exceeds 0.5.

fraction of the step, involves directed diffusion of the TH with anisotropic translational diffusion but isotropic rotational motion.

The final stage, during which the TH attaches to the TBS with proper orientation ($\theta_1 \approx \theta_2 \approx 0$) and with d ≈ 0, can be directed and depends on the strength of the MT-TH interaction, and hence the nucleotide state of the motor head. Upon first entering the neighborhood of the TBS (d ≈ 4 nm), which occurs at the end of the anisotropic diffusive stage, the orientation of the TH with respect to the MT deviates substantially from that found in the Kin-MT complex (Figures 7B–7D; Figure S3). Binding to the TBS with proper orientation could occur either purely by rotational diffusion or can be altered by changing $\varepsilon_h^{MT\text{-}TH}$. In order to distinguish between these two possibilities, we varied the $\varepsilon_h^{MT\text{-}TH}$ from 0.0 to 2.0 kcal/mol. For $\varepsilon_h^{MT\text{-}TH} = 0$, even after entering the neighborhood of the TBS, the TH stochastically samples a broad range of d (see Figure 7B and Figure S3e), θ_1 (Figure 7B and Figure S3f), and θ_2 (Figures S3g and S4a) values. As expected in a purely diffusive process, the TH fluctuates in and out of the neighborhood of the TBS, without forming the required interface with the TBS for a 16 nm step (see Figures S4a–S4c). Thus, in the absence of specific interactions between the motor head and the MT, the TH cannot bind to the αβ-tubulin with substantial probability.

The dynamic behavior for non-zero $\varepsilon_h^{MT\text{-}TH}$ is dramatically different (Figures 7C and 7D; Figure S3). For $\varepsilon_h^{MT\text{-}TH} = 0.2$ Kcal/mol, for which P_{ss} is smallest (Figure 3A), the TH undergoes rotational and translation diffusion even when d ≤ 3 nm (Figure 7C; Figure S4b). The stochastic motion finally ceases only after multiple trials (Figure 7C), resulting in the capture of the TH by the αβ-tubulin, thus completing a full step. In contrast, for $\varepsilon_h^{MT\text{-}TH} = 2.0$ kcal/mol, once the TH approaches the neighborhood of the MT, with both $\theta_1(t)$ and $\theta_2(t)$ appreciably different from zero, the MT-TH interaction is sufficiently strong that orientational ordering occurs rapidly (see Figure 7D and Figure S4c for a representative trajectory), resulting in the rapid cessation of translational and rotational diffusion.

The nature of arrest of translational and rotational diffusion in the final stages of stepping, leading to the capture of the TH by the TBS and completion of the step, illustrates the crucial role played by interaction of the TH with the MT. The rate of orientation arrest depends on the strength of specific interactions between the TH and the TBS (Figures 7B–7D; Figures S4e–S4g). Although several crystal structures (Nitta et al., 2004, 2008) reveal how such interactions are affected by ADP release, when the release occurs during the 16 nm step is unclear. Our simulations point to two mutually conflicting requirements for optimal stepping dynamics. A large value of $\varepsilon_h^{MT\text{-}TH}$ results in rapid orientational ordering of the TH with respect to the TBS. However, the increased rate comes at the expense of enhanced probability of side steps (Figure 3A). When $\varepsilon_h^{MT\text{-}TH} = 0$, the probability of docking to the TBS is zero. Thus, an optimal value of $\varepsilon_h^{MT\text{-}TH}$ leads to the smallest P_{ss} (Figure 3A) and high probability of reaching the TBS, resulting in the correct MT-Kin interface. The importance of MT-Kin interactions in facilitating stepping has been emphasized in a number of experiments (see, for example, Uchimura et al. [2010]).

Conclusions

We have provided detailed simulations of the structural basis of stepping of kinesin on microtubules. Besides the geometrical

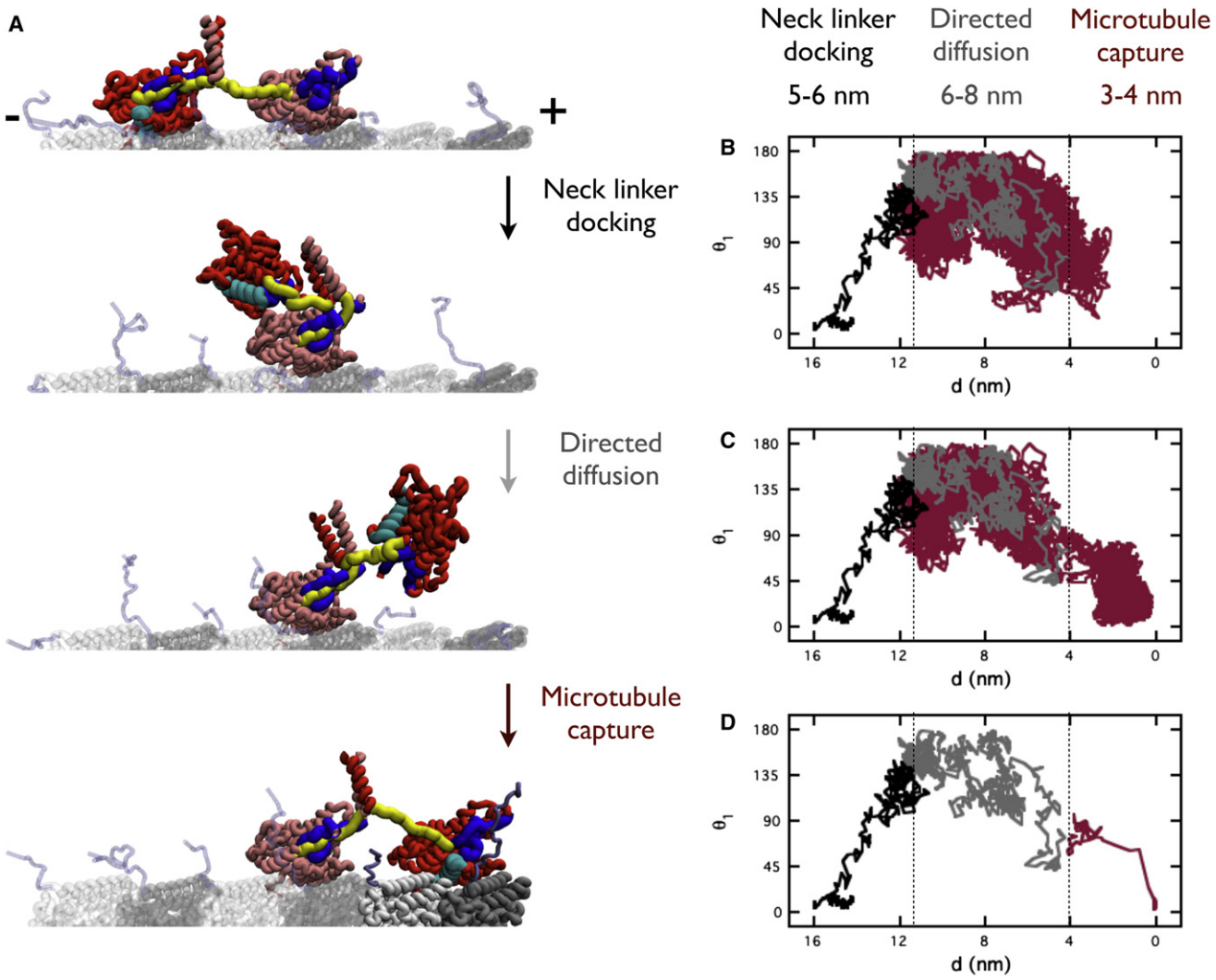

Figure 7. Major Stages during a Single Step

(A) Four snapshots in a representative trajectory, corresponding to (top to bottom) the beginning of the step, the end of neck linker docking to the LH, the end of constrained diffusion, and the end of microtubule capture. Times for the three major steps are indicated. The time for directed diffusion varies from 1.8 to 3.0 μs depending on $\varepsilon_h^{MT\text{-}TH}$, the strength of MT-Kin interaction. The time for binding to the TBS occurs in 5.5 ± 0.6, 1.8 ± 0.4, and 0.5 ± 0.2 μs for $\varepsilon_h^{MT\text{-}TH}$ of 0.2, 0.4, and 2.0 kcal/mol, respectively. Microtubule capture is not observed within 25 μs in simulations with repulsive MT-TH attraction ($\varepsilon_h^{MT\text{-}TH}$ = 0 kcal/mol).

(B–D) Orientation of the TH (θ_1) as a function of d, the center-of-mass distance between the TH and TBS, in three trajectories, in which the MT-TH interaction is repulsive (B), weakly attractive (C), or strongly attractive (D). Each trajectory can be dissected into three stages: neck linker docking (black), constrained diffusion (gray), and microtubule capture (red). A similar plot of θ_2 as a function of d is in Figure S4.

See also Figure S3.

restrictions imposed by the polar track, two energy scales are needed to rationalize the experimental observations. One is the favorable interaction between the neck linker and the motor head required for docking and stretching of the neck linker. The other is the overall interaction between kinesin heads and the microtubule. The former has to exceed a minimum value, while the latter has to have an optimal value to minimize the probability of the TH taking side steps. Our simulations, which provide a molecular description of the events that occur during the jump from one tubulin binding site to another, show that although NL docking to the LH moves the trailing head by less than 6 nm, it not only decreases the probability of the TH taking side steps but also prevents reattachment of the TH to the initial binding site. Therefore, besides directly pulling the motor head toward the target binding site, the power stroke also facilitates motility by regulating diffusion of the motor head so that binding to the target site is favored.

The major findings of our study support the conclusions of a number of single-molecule experiments, which showed that the primary consequences of NL docking are to (1) provide directionality of the TH movement toward the (+) end of the MT (Rice et al., 1999; Yildiz et al., 2008), and (2) serve as a mechanism that prevents excursions of the TH to the neighboring αβ-tubulin binding sites. The present work also substantiates

the importance of directed anisotropic diffusion during 16 nm steps (Schief and Howard, 2001; Block, 2007; Carter and Cross, 2005; Taniguchi et al., 2005). Our work, which also elucidates how optimal interaction between the motor head and the microtubule facilitates motility of kinesin along a single protofilament, has additional implications. (1) Mutations or deletions that affect the MT-TH interaction will impair the processivity of kinesin. This prediction can be tested by mutations in either the MT (Uchimura et al., 2006) or the motor head (Woehlke et al., 1997) and by changing salt concentrations, which would also directly affect $\varepsilon_h^{MT\text{-}TH}$. (2) The enhanced probability of taking side steps, which occurs as the strength of MT-TH interaction increases, suggests that for efficient stepping, ADP release must occur only in the final stages (or after) of the capture of the TH by the MT. In other words, ADP release time, τ_{ADP}, must approximately exceed the stepping time, τ_S. The inequality τ_{ADP} (~ms [Hackney, 1988; Gilbert et al., 1995]) > τ_S (~μs) is satisfied in practice.

EXPERIMENTAL PROCEDURES

Although progress is being made in the use of atomically detailed models to simulate some aspects of molecular motors (Elber and West, 2010; Elber, 2011), the large size of the MT-Kin complex makes it necessary to use coarse-grained models. We performed Brownian dynamics simulations with hydrodynamic interactions using the self-organized polymer (SOP) model for the MT and conventional Kinesin. In the simplest version of the SOP model, each amino acid is represented by a single interaction center located at the α carbon. Previous applications have shown that the SOP model is successful in a number of applications (single-molecule force spectroscopy of proteins [Mickler et al., 2007] and RNA [Hyeon and Thirumalai, 2007], allosteric transitions in the chaperonin GroEL [Hyeon et al., 2006], ATP-induced detachment of myosin V from actin [Tehver and Thirumalai, 2010], and force-induced rupture of αβ-tubulin [Dima and Joshi, 2008; Joshi et al., 2010]). With the SOP representation of the entire system of kinesin, the coiled coil, and the MT, we generated long multiple trajectories, which allow us to obtain a detailed molecular picture of the mechanism that drives the kinesin step. Our construct for the MT-Kin complex, which closely resembles the experimental set-up and builds on a closely related model (Hyeon and Onuchic, 2007a, 2007b), includes two motor heads, a 500 nm bead (cargo), and a 30 nm coiled coil that connects the motor heads to the cargo. We also used three neighboring MT protofilaments in our simulation so that the role of MT in modulating the stepping dynamics can be directly assessed. At t = 0, the TH is bound to the αβ-tubulin at the (−) end of the center protofilament, and the LH is bound to the neighboring αβ-tubulin of the same protofilament (Figure 1C). The LH neck linker (Figure 1C) is undocked (disordered) and points (from T326 to T338) backward toward the MT (−) end, while the TH neck linker (Figure 1C) is docked (ordered), and points forward toward the MT (+) end.

Although we do not explicitly model ATP binding, the consequences of ATP binding and hydrolysis are explicitly taken into account in the simulations. We simulate NL docking induced by ATP binding by changing the interaction between NL and the motor head. Similarly, a weak interaction between the motor head and the binding sites on the microtubule mimics the ADP state. We triggered NL docking at t = 0 in the LH and undocking in the TH and detachment of the TH from the MT (see Supplemental Information for details). After detachment, the TH can reattach to any unoccupied non-minus-end αβ-tubulin binding sites (Figure 1B). We generated a large number of trajectories for 30 μs or longer, which roughly coincides with the duration of jump of the cargo in single-molecule experiments.

We previously described the procedure for obtaining real times from simulations (Veitshans et al., 1997). In order to ensure that this procedure is reasonable, we used simulations to calculate the translational and rotational diffusion constants of an isolated motor head. The simulations were in excellent agreement with the predictions based on HydroPro (García De La Torre et al., 2000), without any adjustable parameter, which shows that the overall timescales associated with our simulations are accurate.

In order to provide structural basis of kinesin stepping we also performed a number of mutation simulations that further reveal how NL docking, characterized by $\varepsilon_h^{LH\text{-}NL}$, affects kinesin motility. Another important parameter that determines the kinematics of the kinesin step is the strength of interaction between kinesin and MT, parameterized by the energy scale $\varepsilon_h^{MT\text{-}TH}$ (see Equation 1 in the Supplemental Information). The affinity of the motor head for αβ-tubulin depends on the state of the nucleotide. Interaction between kinesin and the MT is strongest in the absence of nucleotide or when ATP is bound, and is weak when the motor head carries ADP. Thus, by varying $\varepsilon_h^{MT\text{-}TH}$, which in our simulations is changed from 0.2 to 2.0 kcal/mol, we can roughly mimic the state of the nucleotide. A small value of $\varepsilon_h^{MT\text{-}TH}$ implies that ADP is bound to the TH during the stepping process, whereas $\varepsilon_h^{MT\text{-}TH}$ = 2.0 kcal/mol may correspond to premature release of ADP from the TH.

Analysis of Trajectories

Neck Linker Docking

To assess if the neck linker is in the docked state, we first calculated

$$\Delta_{NL}(t) = \sqrt{\frac{\sum_{(i,j)} \left(r_{ij}(t) - r_{ij}^0\right)^2}{N}}, \quad (1)$$

where i refers to a specific residue in the LH neck linker and j belongs to the docking site, N is the total number of residue pairs that satisfy $r_{ij}^0 < 1$ nm. We used the rat monomeric kinesin structure (PDB code 2kin) to calculate r_{ij}^0. Second, we computed

$$\delta(t) = 1 - \hat{e}_{NL}(t) \cdot \hat{e}_{NL}(d), \quad (2)$$

where $\hat{e}_{NL}(t)$ is the unit vector connecting T326 and T338 in the LH neck linker at time t and $\hat{e}_{NL}(d)$ is the corresponding unit vector in the docked state. If Δ_{NL}(t) and δ(t) are less than preset threshold values Δc and δc then we assume that the neck linker is docked. In most of our simulations we use Δc = 0.08 nm and δc = 0.2. In some cases we also used Δc = 0.06 nm and δc = 0.15 to ensure that the conclusions do not depend on the precise values of Δc and δc (Table S1).

Binding of Motor Head to αβ-Tubulin

We used two order parameters to monitor binding of TH to a specific αβ-tubulin with proper orientation. The first is

$$d(t) = |\vec{r}_{cm}(t) - \vec{r}_{cm}(b)|, \quad (3)$$

where $\vec{r}_{cm}(t)$ is the center-of-mass coordinate of the TH (residues 2–326) at time t, $\vec{r}_{cm}(b)$ is the center of mass coordinate of a motor head docked to a specific αβ-tubulin site as shown in step 2 in Figure S1. The reference state for assessing the correctness of motor head binding to the αβ-tubulin with the similar orientation is the MT-Kin complex structure 2p4n.pdb. The second is the orientational order parameter,

$$\theta_1(t) = cos^{-1}\left(\hat{e}_1(t) \cdot \hat{e}_1(b)\right), \quad (4)$$

where $\hat{e}_1(t)$ is the unit vector connecting L257 and A268 in the TH at t and $\hat{e}_1(b)$ is the corresponding vector in the docked motor head. Similarly, we also considered

$$\theta_2(t) = cos^{-1}\left(\hat{e}_2(t) \cdot \hat{e}_2(b)\right), \quad (5)$$

where $\hat{e}_2(t)$ is the unit vector connecting K227 and K315 in the TH for a given t and $\hat{e}_2(b)$ is the corresponding vector in the docked motor head. If d(t), θ_1(t), and θ_2(t) are smaller than d_c (0.2 nm) and θ_c (15°) then we assume that the TH is bound to the αβ-tubulin with proper orientation.

Probability of Side Steps

From the dynamics of each trajectory, we calculated the total time the motor head spends in the neighborhood of an αβ-tubulin binding site in the protofilament that is adjacent to the one containing the TBS (see Figure 1). The probability of taking a side step is computed using

$$Pss = \frac{\sum \tau_{ss}^i}{\sum \tau_{TBS}^i + \sum \tau_{ss}^i}, \quad (6)$$

where the summation is over all of the trajectories. We assume that the TH is in the neighborhood of the αβ-tubulin binding site if the root-mean-squared deviation (RMSD),

$$\Delta_{TH}(t) = \sqrt{\frac{\sum_{(ij)} \left(R_{ij}(t) - R_{ij}^{0}\right)^{2}}{N}}, \quad (7)$$

between the TH and the binding site is less than 4 nm. In Equation 7, Rij(t) is the distance between residue i in the motor head and residue j in the MT at t and R_{ij}^{0} is the corresponding value in the MT-Kin complex. The summation in Equation 7 is restricted to only values of $R_{ij}^{0} \leq 1$ nm.

SUPPLEMENTAL INFORMATION

Supplemental Information includes four figures, one table, and Supplemental Experimental Procedures and can be found with this article online at doi:10.1016/j.str.2012.02.013.

ACKNOWLEDGMENTS

We are grateful to Dr. K.H. Downing for providing the coordinates of the microtubule. We appreciate interactions with Prof. Michael E. Fisher during the course of this work. We would like to thank S. Chakraborty, G. Reddy, and P. Zhravlev for useful discussions and comments on the manuscript. This work was supported by a grant from the National Science Foundation (CHE 09-14033).

Received: November 26, 2011
Revised: January 19, 2012
Accepted: February 9, 2012
Published: April 3, 2012

REFERENCES

Asbury, C.L., Fehr, A.N., and Block, S.M. (2003). Kinesin moves by an asymmetric hand-over-hand mechanism. Science *302*, 2130–2134.

Asenjo, A.B., Weinberg, Y., and Sosa, H. (2006). Nucleotide binding and hydrolysis induces a disorder-order transition in the kinesin neck-linker region. Nat. Struct. Mol. Biol. *13*, 648–654.

Block, S.M. (2007). Kinesin motor mechanics: binding, stepping, tracking, gating, and limping. Biophys. J. *92*, 2986–2995.

Block, S.M., Asbury, C.L., Shaevitz, J.W., and Lang, M.J. (2003). Probing the kinesin reaction cycle with a 2D optical force clamp. Proc. Natl. Acad. Sci. USA *100*, 2351–2356.

Carter, N.J., and Cross, R.A. (2005). Mechanics of the kinesin step. Nature *435*, 308–312.

Carter, N.J., and Cross, R.A. (2006). Kinesin's moonwalk. Curr. Opin. Cell Biol. *18*, 61–67.

Clancy, B.E., Behnke-Parks, W.M., Andreasson, J.O.L., Rosenfeld, S.S., and Block, S.M. (2011). A universal pathway for kinesin stepping. Nat. Struct. Mol. Biol. *18*, 1020–1027.

Dima, R.I., and Joshi, H. (2008). Probing the origin of tubulin rigidity with molecular simulations. Proc. Natl. Acad. Sci. USA *105*, 15743–15748.

Elber, R. (2011). Simulations of allosteric transitions. Curr. Opin. Struct. Biol. *21*, 167–172.

Elber, R., and West, A. (2010). Atomically detailed simulation of the recovery stroke in myosin by Milestoning. Proc. Natl. Acad. Sci. USA *107*, 5001–5005.

García De La Torre, J., Huertas, M.L., and Carrasco, B. (2000). Calculation of hydrodynamic properties of globular proteins from their atomic-level structure. Biophys. J. *78*, 719–730.

Gennerich, A., and Vale, R.D. (2009). Walking the walk: how kinesin and dynein coordinate their steps. Curr. Opin. Cell Biol. *21*, 59–67.

Gilbert, S.P., Webb, M.R., Brune, M., and Johnson, K.A. (1995). Pathway of processive ATP hydrolysis by kinesin. Nature *373*, 671–676.

Guydosh, N.R., and Block, S.M. (2006). Backsteps induced by nucleotide analogs suggest the front head of kinesin is gated by strain. Proc. Natl. Acad. Sci. USA *103*, 8054–8059.

Hackney, D.D. (1988). Kinesin ATPase: rate-limiting ADP release. Proc. Natl. Acad. Sci. USA *85*, 6314–6318.

Hackney, D.D. (2005). The tethered motor domain of a kinesin-microtubule complex catalyzes reversible synthesis of bound ATP. Proc. Natl. Acad. Sci. USA *102*, 18338–18343.

Hariharan, V., and Hancock, W.O. (2009). Insights into the mechanical properties of the kinesin neck linker domain from sequence analysis and molecular dynamics simulations. Cell Mol. Bioeng. *2*, 177–189.

Hirokawa, N., Noda, Y., Tanaka, Y., and Niwa, S. (2009). Kinesin superfamily motor proteins and intracellular transport. Nat. Rev. Mol. Cell Biol. *10*, 682–696.

Hua, W., Chung, J., and Gelles, J. (2002). Distinguishing inchworm and hand-over-hand processive kinesin movement by neck rotation measurements. Science *295*, 844–848.

Hwang, W., Lang, M.J., and Karplus, M. (2008). Force generation in kinesin hinges on cover-neck bundle formation. Structure *16*, 62–71.

Hyeon, C., and Onuchic, J.N. (2007a). Mechanical control of the directional stepping dynamics of the kinesin motor. Proc. Natl. Acad. Sci. USA *104*, 17382–17387.

Hyeon, C., and Onuchic, J.N. (2007b). Internal strain regulates the nucleotide binding site of the kinesin leading head. Proc. Natl. Acad. Sci. USA *104*, 2175–2180.

Hyeon, C., and Thirumalai, D. (2007). Mechanical unfolding of RNA: from hairpins to structures with internal multiloops. Biophys. J. *92*, 731–743.

Hyeon, C., Lorimer, G.H., and Thirumalai, D. (2006). Dynamics of allosteric transitions in GroEL. Proc. Natl. Acad. Sci. USA *103*, 18939–18944.

Joshi, H., Momin, F., Haines, K.E., and Dima, R.I. (2010). Exploring the contribution of collective motions to the dynamics of forced-unfolding in tubulin. Biophys. J. *98*, 657–666.

Khalil, A.S., Appleyard, D.C., Labno, A.K., Georges, A., Karplus, M., Belcher, A.M., Hwang, W., and Lang, M.J. (2008). Kinesin's cover-neck bundle folds forward to generate force. Proc. Natl. Acad. Sci. USA *105*, 19247–19252.

Kolomeisky, A.B., and Fisher, M.E. (2007). Molecular motors: a theorist's perspective. Annu. Rev. Phys. Chem. *58*, 675–695.

Kozielski, F., Sack, S., Marx, A., Thormählen, M., Schönbrunn, E., Biou, V., Thompson, A., Mandelkow, E.M., and Mandelkow, E. (1997). The crystal structure of dimeric kinesin and implications for microtubule-dependent motility. Cell *91*, 985–994.

Mickler, M., Dima, R.I., Dietz, H., Hyeon, C., Thirumalai, D., and Rief, M. (2007). Revealing the bifurcation in the unfolding pathways of GFP by using single-molecule experiments and simulations. Proc. Natl. Acad. Sci. USA *104*, 20268–20273.

Nitta, R., Kikkawa, M., Okada, Y., and Hirokawa, N. (2004). KIF1A alternately uses two loops to bind microtubules. Science *305*, 678–683.

Nitta, R., Okada, Y., and Hirokawa, N. (2008). Structural model for strain-dependent microtubule activation of Mg-ADP release from kinesin. Nat. Struct. Mol. Biol. *15*, 1067–1075.

Ray, S., Meyhöfer, E., Milligan, R.A., and Howard, J. (1993). Kinesin follows the microtubule's protofilament axis. J. Cell Biol. *121*, 1083–1093.

Rice, S., Lin, A.W., Safer, D., Hart, C.L., Naber, N., Carragher, B.O., Cain, S.M., Pechatnikova, E., Wilson-Kubalek, E.M., Whittaker, M., et al. (1999). A structural change in the kinesin motor protein that drives motility. Nature *402*, 778–784.

Rice, S., Cui, Y., Sindelar, C., Naber, N., Matuska, M., Vale, R.D., and Cooke, R. (2003). Thermodynamic properties of the kinesin neck-region docking to the catalytic core. Biophys. J. *84*, 1844–1854.

Rosenfeld, S.S., Jefferson, G.M., and King, P.H. (2001). ATP reorients the neck linker of kinesin in two sequential steps. J. Biol. Chem. *276*, 40167–40174.

Schief, W.R., and Howard, J. (2001). Conformational changes during kinesin motility. Curr. Opin. Cell Biol. *13*, 19–28.

Sindelar, C.V., and Downing, K.H. (2007). The beginning of kinesin's force-generating cycle visualized at 9-A resolution. J. Cell Biol. *177*, 377–385.

Skiniotis, G., Surrey, T., Altmann, S., Gross, H., Song, Y.H., Mandelkow, E., and Hoenger, A. (2003). Nucleotide-induced conformations in the neck region of dimeric kinesin. EMBO J. *22*, 1518–1528.

Spudich, J.A., and Sivaramakrishnan, S. (2010). Myosin VI: an innovative motor that challenged the swinging lever arm hypothesis. Nat. Rev. Mol. Cell Biol. *11*, 128–137.

Svoboda, K., Schmidt, C.F., Schnapp, B.J., and Block, S.M. (1993). Direct observation of kinesin stepping by optical trapping interferometry. Nature *365*, 721–727.

Taniguchi, Y., Nishiyama, M., Ishii, Y., and Yanagida, T. (2005). Entropy rectifies the Brownian steps of kinesin. Nat. Chem. Biol. *1*, 342–347.

Tehver, R., and Thirumalai, D. (2010). Rigor to post-rigor transition in myosin V: link between the dynamics and the supporting architecture. Structure *18*, 471–481.

Tomishige, M., and Vale, R.D. (2000). Controlling kinesin by reversible disulfide cross-linking. Identifying the motility-producing conformational change. J. Cell Biol. *151*, 1081–1092.

Tomishige, M., Stuurman, N., and Vale, R.D. (2006). Single-molecule observations of neck linker conformational changes in the kinesin motor protein. Nat. Struct. Mol. Biol. *13*, 887–894.

Uchimura, S., Oguchi, Y., Katsuki, M., Usui, T., Osada, H., Nikawa, J., Ishiwata, S., and Muto, E. (2006). Identification of a strong binding site for kinesin on the microtubule using mutant analysis of tubulin. EMBO J. *25*, 5932–5941.

Uchimura, S., Oguchi, Y., Hachikubo, Y., Ishiwata, S., and Muto, E. (2010). Key residues on microtubule responsible for activation of kinesin ATPase. EMBO J. *29*, 1167–1175.

Vale, R.D. (2003). The molecular motor toolbox for intracellular transport. Cell *112*, 467–480.

Vale, R.D., and Milligan, R.A. (2000). The way things move: looking under the hood of molecular motor proteins. Science *288*, 88–95.

Veitshans, T., Klimov, D., and Thirumalai, D. (1997). Protein folding kinetics: timescales, pathways and energy landscapes in terms of sequence-dependent properties. Fold. Des. *2*, 1–22.

Woehlke, G., Ruby, A.K., Hart, C.L., Ly, B., Hom-Booher, N., and Vale, R.D. (1997). Microtubule interaction site of the kinesin motor. Cell *90*, 207–216.

Yildiz, A., Tomishige, M., Vale, R.D., and Selvin, P.R. (2004). Kinesin walks hand-over-hand. Science *303*, 676–678.

Yildiz, A., Tomishige, M., Gennerich, A., and Vale, R.D. (2008). Intramolecular strain coordinates kinesin stepping behavior along microtubules. Cell *134*, 1030–1041.

